coatings

MDPI

Article

Heat Transfer Analysis of Unsteady MHD Carreau Fluid Flow over a Stretching/Shrinking Sheet

Mubashir Qayyum [1], Tariq Abbas [2], Sidra Afzal [1], Syed Tauseef Saeed [1], Ali Akgül [3,4,*], Mustafa Inc [5,6,*], Khaled H. Mahmoud [7] and Abdullah Saad Alsubaie [7]

1 Department of Sciences and Humanities, National University of Computer and Emerging Sciences, Lahore 54770, Pakistan
2 Department of Mathematics, Faculty of Sciences, Sarhad University of Science and Information Technology, Peshawar 25000, Pakistan
3 Department of Mathematics, Art and Science Faculty, Sirt University, Sirt 56100, Turkey
4 Mathematics Research Center, Department of Mathematics, Near East University, Near East Boulenvard, Nicosia 99138, Turkey
5 Department of Mathematics, Firat University, Elazig 23119, Turkey
6 Department of Medical Research, China Medical University, Taichung 40402, Taiwan
7 Department of Physics, College of Khurma University College, Taif University, P.O. Box 11099, Taif 21944, Saudi Arabia
* Correspondence: aliakgul@siirt.edu.tr (A.A.); minc@firat.edu.tr (M.I.)

Abstract: This manuscript contains the modeling and analysis of an unsteady Carreau fluid with a magnetohydrodynamical effect over a stretching sheet. The governing momentum and energy equations admit a self-similarity solution. The system of ordinary differential equations has been solved analytically by the homotopy analysis method (HAM) and numerically by BVP4C (Matlab routine). An analysis of results shows that obtained analytical and numerical solutions are in excellent agreement with existing results in the literature. Furthermore, the effect of various fluid parameters on the velocity and temperature profiles are studied graphically. It is observed that velocity increases in the stretching sheet for power law index n and the Weissenberg number We, whereas it decreases for magnetic parameter M^2. Tabular analysis on skin friction and heat transfer rate is also presented against pertinent fluid parameters.

Keywords: boundary layer; stagnation point flow; suction/injection; stretching/shrinking sheet

Citation: Qayyum, M.; Abbas, T.; Afzal, S.; Saeed, S.T.; Akgül, A.; Inc, M.; Mahmoud, K.H.; Alsubaie, A.S. Heat Transfer Analysis of Unsteady MHD Carreau Fluid Flow over a Stretching/Shrinking Sheet. *Coatings* **2022**, *12*, 1661. https://doi.org/10.3390/coatings12111661

Academic Editor: Eduardo Guzmán

Received: 27 September 2022
Accepted: 27 October 2022
Published: 1 November 2022

1. Introduction

The study of boundary-layer flow over a stretching or shrinking surface with heat transfer has received a lot of attention from several scientists due to its enormous potential for application in engineering and industry. The existence of the boundary layer is subject to relative motion of the fluid and solid surface where fluid is in contact. Specific examples include the extrusion of plastic sheets and polymers in the melt spinning process, the production of glass fibers and plastic films, wire drawing, hot rolling, and paper production etc. Sakiadis [1] examined the behavior of boundary layer flow over a constant solid surface that moves at constant speed. Crane [2] studied the flow of the boundary layer past a stretching sheet where distance from the slit is proportional to the velocity. The effect of suction and blowing with heat and mass transfer in a boundary layer over a stretching surface is investigated by Gupta et al. [3]. Rasheed et al. [4] analyzed a Jeffery nanofluid passing over a vertically stretched cylinder under magnetohydrodynamic effect. In order to check stability and convergence of the fluid model, the homotopy analysis method was employed. Kalpana and Saleem [5] investigated dusty fluid flows under magnetohydrodynamic effects in an irregular porous channel. They employed the finite difference algorithm to solve the flow problem. Stability analysis with dual solutions for a Casson fluid flow over a stretching surface is done by Hamid et al. [6]. Inayat et al. [7]

studied magnetohydrodynamic squeezing flows in a porous medium by using homotopy analysis method for solution purposes. Kumar et al. [8] analyzed the flow of a magnetic dipole Maxwell fluid on a stretching surface with thermophoretic particle distribution. A numerical study on a hybrid nanofluid with Newtonian heating on a curved sheet with a stretching effect is characterized by Mudhukesh et al. [9]. Wang [10] examined 2D stagnation point flow with heat transfer over a shrinking/stretching sheet. Qayyum et al. [11] presented slip analysis for Casson fluid flow under a magnetohydrodynamic effect. They utilized a homotopy perturbation scheme to solve a fourth-order differential equation of the flow problem. Raza [12] investigated the flow of Casson fluid with velocity and thermal slip over a stretching sheet near the stagnation point. Patel et al. [13] discussed the transfer of heat into a non-Newtonian 2D stagnation point flow. Ramesh et al. [14] examined the time-dependent squeezing flow of a Cassson micropolar nanofluid with suction/injunction and slip effects on velocity, temperature, and concentration. The unsteady flow of a hybrid nanofluid is analyzed by Waini et al. [15] with heat transfer over a sheet with varied thickness. Khan et al. [16] numerically solved the Carreau fluid flow past a stretching sheet of variable thickness with MHD effect. Akber et al. [17] presented a stretching sheet with the boundary layer stagnation point flow of a Carreau fluid. In the presence of homogeneous and heterogeneous reactions, Raju et al. [18] studied the effects of nonlinear thermal radiation and a nonuniform heat source or sink in unsteady 3D flows of Carreau and Casson fluids past stretching surfaces. Shabnam et al. [19] numerically investigated the squeezing flow between two concentric circles with magnetic field and heat source. Ali et al. [20] presented mathematical modeling for the flow of an incompressible Carreau fluid in an asymmetric channel with variations in the sinusoidal wall. Transport phenomenon on Carreau fluid is studied by Nazir et al. [21] by using the Catteno–Christov heat flux with diffusion coefficients dependent on temperature. Nadeem et al. [22] studied unsteady Carreau fluid flow in eccentric cylinders.

Stretching and shrinking sheets are of much importance in many fields of science, engineering, and physics. For this reason, it encourages many researchers to model and simulate problems based on varying fluid flows past stretching/shrinking surfaces. Kashi'ie et al. [23] studied hybrid nanofluid flow in three dimensions over a variably thickened sheet with convective and slip boundary conditions. Gopal et al. [24] analyzed micropolar fluid flow over a porous shrinking sheet by using the variational finite element method. The flow of a hybrid nanofluid over a permeable shrinking sheet is analyzed by Abu Bakar et al. [25] with the impact of radiation and slip. Rohni et al. [26] investigated the unsteady flow of a water-based nanofluid over a shrinking surface with wall mass suction. Warke et al. [27] numerically analyzed magneto-micropolar liquid flow on a heated and porous stretching sheet. Elbashbeshy et al. [28] obtained a similarity solution of unsteady laminar boundary layer stretching surface flow. The second-grade nanofluid flow past a stretching sheet with impact of the magnetic field is scrutinized by Hayat et al. [29]. By using the finite element approach, Khan et al. [30] characterized micropolar-based nanofluids near a stagnation point flowing past a vertically stretching sheet. Waini et al. [31] considered dusty flow of a hybrid nanofluid on a stretching sheet under the effect of a magnetic field. Hassnian et al. [32] have studied the unsteady mixed convection boundary layer flow near the stagnation point on a heated vertical plate. In the presence of thermal radiation in an unsteady boundary layer flow, Nandy et al. [33] analyzed the forced convection of nanofluid into a permeable shrinking sheet. Zainal et al. [34] did stability analysis on MHD flow of a hybrid nanofluid on a sheet with variable thickness. Heat and mass transport on Carreau nanomaterial near a stagnation point is examined by Chu et al. [35] by using the RK Fehlberg technique. Ahmed et al. [36] explored the flow of a Maxwell nanofluid near the stagnation point on a rotating disk with a heat source/sink. Nik Long et al. [37] investigated an unsteady stagnation point flow and heat transfer over a stretch sheet. Jakeer and Reddy [38] studied entropy generation for a nanofluid near the electro-magnetohydrodynamic stagnation point. Khan et al. [39] analyzed a hybrid nanofluid passing over a non-isothermal stretching surface under the effect of a magnetic

field normal to the surface. Mousavi et al. [40] simulated Casson hybrid nanofluid flow over a stretching shrinking sheet through dual solution model.

The main aim of this manuscript is to model and analyze the unsteady, incompressible boundary layer flow of an MHD Carreau fluid near a stagnation point. In light of the literature review stated above, it is observed that the unsteady Carreau fluid model with boundary layer flow under magnetohydrodynamic effect and suction/injuction is not studied comparatively for stretching/shrinking sheet cases. Moreover, to elaborate the novelty of the current study and the research gap it fills, recent studies on Carreau fluid flow are compared with this manuscript in Table 1. This flow is modeled with magneto-hydrodynamic effect and heat flux. The system of PDEs are transformed into ODEs by using suitable similarity transformations. The obtained system is solved analytically by HAM and numerically by BVP4C. The effect of various fluid parameters on the velocity and temperature profile is analyzed graphically in the case of the stretching and shrinking sheet, comparatively. In addition, the skin friction coefficient and heat transfer rate at sheet surface is tabulated and analyzed. This study is further classified into the following sections: Section 2 presents formulation of flow problem. In Section 3, the homotopy analysis method is used to solve the problem. In Section 4, a discussion and analysis of results is presented, and finally conclusions are drawn in Section 5.

Table 1. Present study in comparison to studies in the literature.

	Unsteady	Boundary Layer	Stagnation Point	Suc./ Inj.	Stretch./ Shrink.	HAM vs. BVP4C
Hayat et al. [41]	No	No	No	No	No	No
Hussain et al. [42]	No	No	No	No	Yes	No
Abbas et al. [43]	No	Yes	Yes	No	Yes	No
Raza et al. [44]	No	No	No	No	Yes	No
Present	Yes	Yes	Yes	Yes	Yes	Yes

2. Problem Formulation

In this study, a Carreau fluid stagnation point flow is considered. The flow is unsteady, incompressible, and two-dimensional on a sheet with stretching/shrinking effect at surface $y = 0$. Moreover, the velocity profile is influenced by magnetohydrodynamic effect in perpendicular direction to sheet surface along with the impact of heat flux in the temperature profile. Flow geometry of the problem is depicted in Figure 1. The governing equations of described flow geometry are modeled as follows [45]:

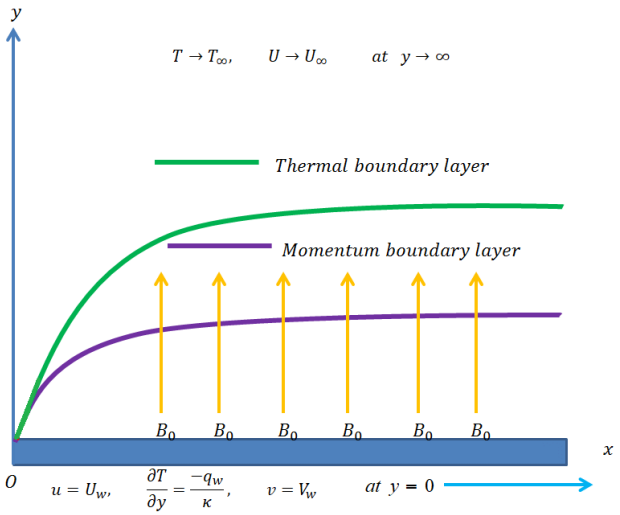

Figure 1. Flow geometry.

$$\nabla.V = 0 \tag{1}$$

$$\frac{\partial u}{\partial t} - \nu\frac{\partial^2 u}{\partial y^2} + u\frac{\partial u}{\partial x} - \frac{\sigma J^2}{\rho}(U_\infty - u) + v\frac{\partial u}{\partial y} - U_\infty\frac{\partial U_\infty}{\partial x} - \frac{3}{2}\nu\Gamma^2(n-1)\frac{\partial^2 u}{\partial y^2}\left(\frac{\partial u}{\partial y}\right)^2 - \frac{\partial U_\infty}{\partial t} = 0, \tag{2}$$

$$u\frac{\partial T}{\partial x} + \frac{\partial T}{\partial t} + v\frac{\partial T}{\partial y} - \alpha\frac{\partial^2 T}{\partial y^2} = 0. \tag{3}$$

The boundary conditions are

$$u(0) = U_w(x,t),\ \frac{\partial T(0)}{\partial y} = -\frac{q_w}{\kappa},\ v(0) = V_w, \tag{4}$$

$$T(\infty) \longrightarrow T_\infty \quad ,\ u(\infty) \longrightarrow U_\infty. \tag{5}$$

In Equations (1)–(5), u is velocity in the x-direction, and v is in the y-direction. Here, ρ is the density of fluid, g is the gravitational acceleration, σ is the electric conductivity, ν is the kinematic viscosity, α is the thermal diffusivity, T_∞ is the ambient temperature, n is the power law index, J is the magnetic field, Γ is the time constant, T_∞ is the ambient temperature, V_w is the suction/injuction parameter, and κ is the thermal conductivity. Moreover, the ambient velocity U_∞, the stretching/shrinking sheet velocity U_w, and surface heat flux q_w are defined as

$$q_w(x,t) = cx(1-\lambda t)^{-1}, \quad U_w(x,t) = bx(1-\lambda t)^{-1}, \quad U_\infty(x,t) = ax(1-\lambda t)^{-1}. \tag{6}$$

In order to simplify system of PDEs in Equations (1)–(5) to system of non-dimensional ODEs, we introduce similarity transformations as

$$\psi = \frac{(a\nu)^{\frac{1}{2}}}{(1-\lambda t)^{\frac{1}{2}}}xf(\xi),\ \xi = \frac{y}{\sqrt{1-\alpha t}}\sqrt{\frac{a}{\nu}},\ \theta(\xi) = \frac{k(T-T_\infty)}{q_w}\sqrt{\frac{U_\infty}{\nu x}}, \tag{7}$$

where u and v are defined as $u = \frac{\partial \psi}{\partial y}$ and $v = -\frac{\partial \psi}{\partial x}$, respectively. By using this u and v in Equation (6), we obtain following transformations:

$$u = \frac{y}{(1-\alpha t)}f'(\xi),\ v = -\frac{(a\nu)^{\frac{1}{2}}}{(1-\lambda t)^{\frac{1}{2}}}f(\xi). \tag{8}$$

By using Equations (6) and (7) in Equations (1)–(5), a nondimensional system is obtained,

$$f''' + \frac{3}{2}We^2(n-1)f'''(f'')^2 - A\frac{\xi f''}{2} + ff'' + 1 - Af' + A - f'^2 - M^2f' + M^2 = 0, \tag{9}$$

$$\frac{1}{Pr}\theta'' - \frac{A\theta}{2} + f\theta' - \xi\frac{A\theta'}{2} - f'\theta = 0, \tag{10}$$

with dimensionless conditions at boundary as

$$\theta'(0) = -1, \quad f'(0) = B, \quad f(0) = S, \tag{11}$$

$$f'(\infty) = 1, \quad \theta(\infty) = 0. \tag{12}$$

In Equations (8)–(10), M^2, We^2, S, A, B, and Pr are the magnetic parameter, Weissenberg number, suction/injuction parameter, unsteadiness parameter, stretching/shrinking parameter, and Prandtl number, respectively. We have

$$M^2 = \frac{\sigma J_0^2(1-\lambda t)}{\rho b}, \quad We^2 = \frac{\Gamma^2 a^3 x^2}{\nu(1-\lambda t)^3}, \quad A = \frac{\lambda}{a}, \quad S = -\frac{V_w(1-\lambda t)^{\frac{1}{2}}}{(av)^{\frac{1}{2}}}, \quad Pr = \frac{\nu}{\alpha}, \quad B = \frac{b}{a}. \tag{13}$$

Quantities of Physical Interest

Skin friction C_f and Nusselt number Nu_x are quantities of physical interest, as defined below,

$$C_f = \frac{\check{\tau}_w}{\rho U_\infty^2/2}, \quad Nu_x = \frac{x\check{q}_w}{\kappa(T-T_\infty)}, \tag{14}$$

where $\check{\tau}_w$ is the stress tensor and $\check{q}_w$ is the heat flux at wall, defined as

$$\check{\tau}_w = \mu\left(\frac{\partial u}{\partial y}\right)_{y=0}, \quad \check{q}_w = -\kappa(\left(\frac{\partial T}{\partial y}\right)_{y=0}. \tag{15}$$

By using Equation (14) in Equation (13) and by using similarity transforms on resulting equations, the nondimensional skin friction and Nusselt number is obtained,

$$C_f = 2Re_x^{-\frac{1}{2}} f''(0), \quad Nu_x = \frac{Re_x^{\frac{1}{2}}}{\theta(0)}, \tag{16}$$

where $R_e(x)$ is the local Reynold number given as $R_e(x) = \frac{U_\infty x}{\nu}$.

3. Homotopy Analysis Solution of the Problem

In this section, the implication of homotopy analysis method on the flow problem is elaborated. Obtained system of ODEs in Equations (8) and (9) with boundary conditions in Equations (10) and (11) are solved by using HAM. We first select the linear operator and initial guess as

$$f_0(\xi) = \xi + (1-B)e^{-\xi} + (S-1+B), \quad \theta_0(\xi) = e^{-\xi}, \tag{17}$$

$$\tilde{L}_f = f'''(\xi) + f''(\xi), \quad \tilde{L}_\theta = \theta''(\xi) + \theta'(\xi). \tag{18}$$

The following properties of the above auxiliary linear operators are

$$\begin{aligned} &\tilde{L}_f(c_1\xi + c_2e^{-\xi} + c_3) = 0, \\ &\tilde{L}_\theta(c_4e^{-\xi} + c_5) = 0, \end{aligned} \tag{19}$$

where $c_i (i = 1(1)5)$ are arbitrary constants. By using initial guess and auxiliary linear operator, the zeroth-order deformation equation becomes

$$(1-q)\tilde{L}_f\check{f}(q;\xi) - qh_f\tilde{N}_f[\check{f}(q;\xi)] - (1-q)\tilde{L}_f f_0(\xi) = 0, \tag{20}$$

$$(1-q)\tilde{L}_\theta\check{\theta}(q;\xi) - qh_\theta\tilde{N}_\theta[\check{\theta}(q;\xi), \check{f}(q;\xi)] - (1-q)\tilde{L}_\theta\theta_0(\xi) = 0. \tag{21}$$

The nonlinear operators are given in following equation:

$$\begin{aligned} \tilde{N}_f[\check{f}(q;\xi)] = {} & \frac{\partial^3\check{f}(q;\xi)}{\partial\xi^3} + A + 1 - A\left[\frac{\partial\check{f}(q;\xi)}{\partial\xi} + \frac{\xi}{2}\frac{\partial^2\check{f}(q;\xi)}{\partial\xi^2}\right] + \frac{\partial^2\check{f}(q;\xi)}{\partial\xi^2}\check{f}(q;\xi) - \left(\frac{\partial\check{f}(q;\xi)}{\partial\xi}\right)^2 \\ & + \frac{3(n-1)}{2}We^2\left(\frac{\partial\check{f}(q;\xi)}{\partial\xi}\right)^2\frac{\partial^3\check{f}(q;\xi)}{\partial\xi^3} + M^2\left[1 - \left(\frac{\partial\check{f}(q;\xi)}{\partial\xi}\right)\right], \end{aligned} \tag{22}$$

$$\tilde{N}_\theta[\check{\theta}(q;\xi), \check{f}(q;\xi)] = \frac{\partial^2\check{\theta}(q;\xi)}{\partial\xi^2} + Pr\check{f}(q;\xi)\frac{\partial\check{\theta}(q;\xi)}{\partial\xi} - A\left(\frac{\check{\theta}(q;\xi)}{2} + \frac{\xi}{2}\frac{\partial\check{\theta}(q;\xi)}{\partial\xi}\right) - Pr\frac{\partial\check{f}(q;\xi)}{\partial\xi}\check{\theta}(q;\xi), \tag{23}$$

where h_f and h_θ are the auxiliary parameters, $\tilde{N}_f$, $\tilde{N}_\theta$ and q are the nonlinear operators and the embedding parameter, respectively. As q varies from 0 to 1, the initial guess transforms to exact solution. We have

$$\begin{aligned} f_0(\xi) &= \breve{f}(0;\xi), \quad f(\xi) = \breve{f}(1;\xi), \\ \theta_0(\xi) &= \breve{\theta}(0;\xi), \quad \theta(\xi) = \breve{\theta}(1;\xi). \end{aligned} \tag{24}$$

Functions $f(\xi;q)$ and $\theta(\xi;q)$ are written after Taylor series expansion as

$$\begin{aligned} f(q;\xi) &= \sum_{k=1}^{\infty} q^k f_k(\xi) + f_0(\xi), \\ \theta(q;\xi) &= \sum_{k=1}^{\infty} q^k \theta_k(\xi) + \theta_0(\xi), \end{aligned} \tag{25}$$

where

$$\begin{aligned} f_k &= \frac{1}{k!}\left(\frac{\partial^k f(q;\xi)}{\partial \xi^k}\right)_{q=0}, \\ \theta_k &= \frac{1}{k!}\left(\frac{\partial^k \theta(q;\xi)}{\partial \xi^k}\right)_{q=0}. \end{aligned} \tag{26}$$

Equation (22) converges for $q = 1$, so we write

$$\begin{aligned} f(\xi) &= \sum_{k=1}^{\infty} f_k(\xi) + f_0(\xi), \\ \theta(\xi) &= \sum_{k=1}^{\infty} \theta_k(\xi) + \theta_0(\xi). \end{aligned} \tag{27}$$

After differentiating the zeroth-order deformation equation k times, we arrive at the following deformation equation of the k-th order,

$$\tilde{L}_f[f_k(\xi) - \chi_k f_{k-1}(\xi)] = h_f \tilde{R}_{f,k}(\xi), \tag{28}$$

$$\tilde{L}_\theta[\theta_k(\xi) - \chi_k \theta_{k-1}(\xi)] = h_\theta \tilde{R}_{\theta,k}(\xi), \tag{29}$$

where

$$\begin{aligned} \tilde{R}_{f,k}(\xi) &= \frac{\partial^3 f_{k-1}(\xi)}{\partial \xi^3} + \sum_{j=0}^{k-1} f_{k-1-j}(\xi)\frac{\partial^2 f_j(\xi)}{\partial \xi^2} - A\left[\frac{\partial f_{k-1}(\xi)}{\partial \xi} + \frac{\xi}{2}\frac{\partial^2 f_{k-1}(\xi)}{\partial \xi^2}\right] - M^2\frac{\partial f_{k-1}(\xi)}{\partial \xi} \\ &+ \frac{3(n-1)}{2}We^2\sum_{j=0}^{k-1}\left[\frac{\partial^2 f_{k-1-j}(\xi)}{\partial \xi^2}\frac{\partial^2 f_k(\xi)}{\partial \xi^2}\right]\frac{\partial^3 f_{k-1}(\xi)}{\partial \xi^3} - \sum_{j=0}^{k-1}\frac{\partial f_{k-1-j}(\xi)}{\partial \xi}\frac{\partial f_k(\xi)}{\partial \xi} + (M^2 + A + 1)(1 - \chi_k), \\ \tilde{R}_{\theta,k}(\xi) &= \frac{\partial^2 \theta_{k-1}(\xi)}{\partial \xi^2} + Pr\sum_{j=0}^{k-1} f_{k-1-j}(\xi)\frac{\partial \theta_k(\xi)}{\partial \xi} - A\left[\frac{\theta_k(\xi)}{2} + \frac{\xi}{2}\frac{\partial \theta_{k-1}(\xi)}{\partial \xi}\right] - Pr\sum_{j=0}^{k-1}\frac{\partial f_{k-1-j}(\xi)}{\partial \xi}\theta_k(\xi), \\ \chi_k &= \begin{cases} 1 & k > 1, \\ 0 & k \leq 1. \end{cases} \end{aligned}$$

Equations (10) and (11), after using Equation (24), gives

$$\begin{aligned} f_k(0) &= f_k^{'}(0) = f_k^{'}(\infty), \\ \theta_k'(0) &= 0 = \theta_k(\infty). \end{aligned} \tag{30}$$

The general solution can be written as

$$f_k(\xi) = f_k^* + c_1\xi + c_2 e^{-\xi} + c_3,$$
$$\theta_k(z) = \theta_k^* + c_4 e^{-\xi} + c_5, \tag{31}$$

where f_k^*, and θ_k^* are the special solutions.

4. Analysis of Results

In this section, we analyze the flow behavior of the Carreau fluid under the effects of MHD and heat flux on the stretching and shrinking sheet comparatively. Numerical and analytical analysis is done on nonlinear ODEs (8) and (9) by using BVP4C and the homotopy analysis method. Graphical results are obtained for velocity and temperature profile for various fluid parameters. Figure 2 shows effects of various nondimensional parameters on the velocity profile. The effect of the Weissenberg number, We on velocity $f'(\xi)$ is illustrated in Figure 2a. We decreases velocity of the fluid when the sheet is shrinking. The opposite behavior of We on the velocity profile is observed for the stretching sheet case. An increase in We decreases fluid viscosity, resulting in increased fluid velocity for the stretching sheet. Figure 2b presents the power law index, n against velocity $f'(\xi)$. With an increase in n, velocity increases in the case of the stretching sheet, whereas it decreases for the shrinking sheet case. The unsteadiness parameter A increases velocity distribution in the shrinking case, as seen in Figure 2c. In Figure 2d, the effect of the suction/injuction parameter S on velocity is shown. An increase in axial velocity of fluid is observed with increasing rate of stretching. As S increases, more fluid flow is caused in the axial direction due to suction/injuction. The effect of magnetic interaction parameter M on velocity is depicted in Figure 2e. In the case of the shrinking sheet, velocity increases with an increase in M, and it decreases when the sheet is stretching. Increased M results in Lorentz-like drag force, which causes resistance in fluid flow when the sheet stretches. The behavior of the temperature profile for the Prandtl number Pr and unsteadiness parameter A is shown in Figure 2. When the Prandtl number, Pr is increased in Figure 3a, it is observed that fluid temperature depreciates due to decreased thermal diffusivity. The unsteadiness parameter A decreases temperature, $\theta\xi$ in Figure 3b. A is increased whereas Pr is kept constant. Table 2 depicts numerical results for skin friction coefficient $f''(0)$ and Nusselt number $\frac{1}{\theta(0)}$ for increasing values of various parameters. Analysis reveals that increasing n for the stretching sheet elevates skin friction and Nusselt number. A decrease in skin friction and heat transfer rate against n is observed for the shrinking sheet case. The suction parameter S is increased with the stretching/shrinking parameter, $B = 0, 3$. The skin friction and heat transfer rate boosts as S is increased. Increasing values of magnetic interaction parameter, M^2 show varying results in the stretching and shrinking case. When the stretching sheet is considered, skin friction and heat transfer rate decrease with increasing values of M^2, whereas the opposite behavior is observed in case of the shrinking sheet. The increasing unsteadiness parameter A elevates skin friction and heat transfer in both cases of shrinking and stretching. Moreover, for the stretching sheet, skin friction and heat transfer is increased for higher values of the Weissenberg number We, whereas contrasting results are noted in case shrinking sheet. The numerical results of $-\theta'(\xi)$, $f(\xi)$, $f'(\xi)$ and $f''(\xi)$ are tabulated in Table 3. The results obtained from HAM are observed to be in good agreement with BVP4C results depicting validity of obtained solution. Moreover, the validity of the solution is also confirmed by comparison of results with Wang [10], M. Sauli et al. [46], and Nik Long [37] for $A = 0, 0.1$ with varying values of B (see Tables 4 and 5).

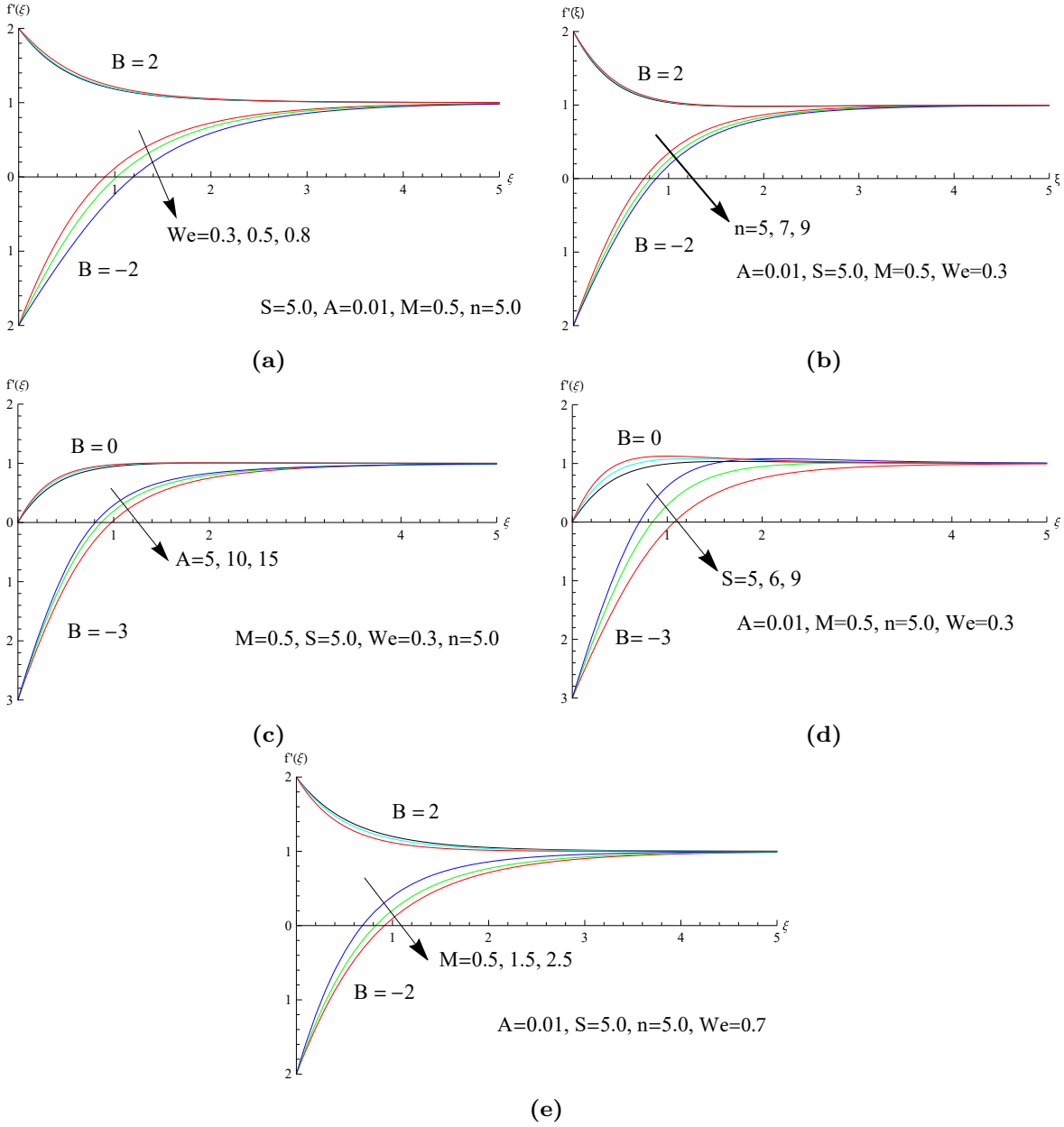

Figure 2. Behavior of velocity profile against pertinent fluid parameters. (**a**) variation of We; (**b**) variation of n; (**c**) variation of A; (**d**) variation of S; (**e**) variation of M.

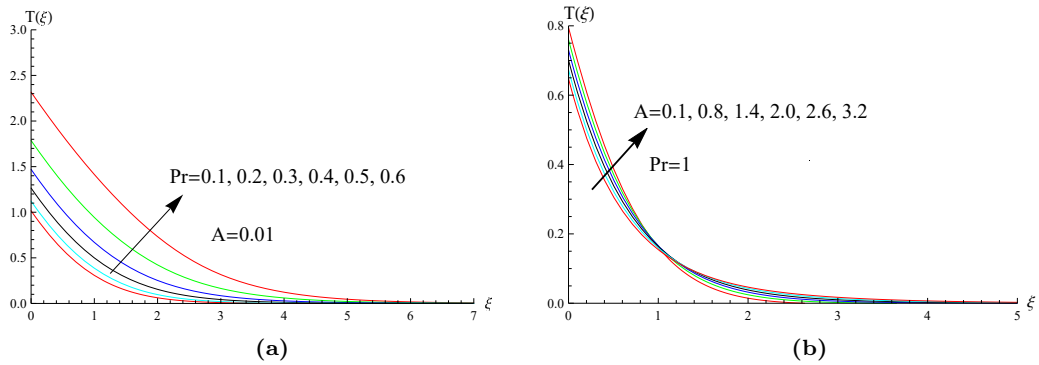

Figure 3. Behavior of temperature profile against pertinent fluid parameters. (**a**) variation of Pr; (**b**) variation of A.

Table 2. Skin friction and Nusselt number at wall, $\xi = 0$.

B	n	S	A	M	We	$\frac{1}{\theta(0)}$	$f''(0)$
2.0	5.0					4.0244430	−2.6826278
	6.0					4.0283364	−2.5369399
	7.0					4.0315875	−2.4219666
−2.0	5.0					3.0481391	3.8906419
	6.0					3.0252388	3.6346990
	7.0					3.0062235	3.4364046
0.0	5.0	5.0				3.6630343	2.5611289
		5.5				3.9971591	2.6619630
		6.0				4.3335662	2.7577551
−3.0		5.0				2.5696252	4.0561451
		5.5				3.0065323	4.2665821
		6.0				3.4264443	4.4570918
0.0			0.5			3.6674852	2.5762846
			1.0			3.6723614	2.5916306
			1.5			3.6776320	2.6068546
−3.0			0.5			2.5721711	4.1243391
			1.0			2.5765875	4.1918215
			1.5			2.5835476	4.2573624
2.0			0.01	5.0		4.0042851	−3.4638604
				6.0		3.9992199	−3.6839415
				7.0		3.9944856	−3.9006953
−2.0				5.0		3.1749996	5.7788121
				6.0		3.1989911	6.2168226
				7.0		3.22032152	6.6343644
2.0					0.5	4.0428543	−2.06140876
					1.4	4.0782778	−1.1683032
					1.8	4.0854061	−1.0139622
−2.0					0.5	2.9401264	2.8342074
					1.4	2.6966604	1.44553072
					1.8	2.6272086	1.2183288

Table 3. Numerical comparison of HAM with BVP4C.

ξ	$f(\xi)$ **Analytical**	$f(\xi)$ **Numerical**	$f'(\xi)$ **Analytical**	$f'(\xi)$ **Numerical**	$f''(\xi)$ **Analytical**	$f''(\xi)$ **Numerical**	$-\theta'(\xi)$ **Analytical**	$-\theta'(\xi)$ **Numerical**
0.004504	0.4022613	0.402261	0.5040192	0.504019	0.8892286	0.889211	0.9970712	0.997067
0.013513	0.4068379	0.406838	0.5119757	0.511976	0.877124	0.8771417	0.9911961	0.991185
0.022527	0.4114857	0.411486	0.5198240	0.519824	0.8651878	0.865170	0.9852988	0.985279
0.031531	0.4162038	0.416204	0.5275651	0.527565	0.8533656	0.853348	0.9793806	0.979353
0.040540	0.4209911	0.420991	0.5352004	0.535200	0.8416738	0.841656	0.9734423	0.973407

Table 4. Comparison of $f''(0)$ when $A = 0$ and $A = 0.1$.

B	A	Present Work	Wang [10]	M. Suali et al. [46]	Nik Long et al. [37]
4.0	0.0	−7.0863775	-	−7.086378	-
3.0		−4.2765414	-	−4.276545	-
0.2		1.0511299	1.05113	1.051130	-
0.1		1.1465607	1.14656	1.146561	-
−0.2		1.3738858	-	1.373886	-
−0.5		1.4956699	1.49567	1.495672	-
−1.15		1.0822445	1.08223	1.082232	-
4.0	0.1	−7.1300170	-	−7.130017	−7.130017
3.0		−4.3087131	-	−4.308713	-
0.2		1.0723284	-	1.072329	1.072329
0.1		1.1711930	-	1.171193	1.171193
−0.2		1.4106490	-	1.410656	-
−0.5		1.5489907	-	1.549006	1.549006
−1.15		1.2549492	-	1.255264	-

Table 5. Comparison of $\frac{1}{\theta(0)}$ when $A = 0$.

B	Present Value	M. Suali et al. [46]	Wang [10]
3.0	1.8706705	1.870671	-
0.2	0.9133029	0.913303	0.91330
0.1	0.8634515	0.863452	0.86345
−0.2	0.6987483	0.698748	0.69875
−0.5	0.5014488	0.501448	0.50145
−1.15	−0.2979289	−0.2979953	−0.29799

5. Conclusions

This study presents solutions and analyses of stagnation point flow of a MHD Carreau fluid with heat flux in the presence of heat transfer. The effects of stretching and shrinking cases of the sheet are analyzed comparatively on velocity profile, temperature profile, skin friction, and heat transfer rate. An increase in velocity profile is observed for increasing values of n and We when the sheet stretches, whereas a decrease in velocity is observed in cases where the sheet shrinks. However, the opposite behavior is observed in case of increasing M^2. Similarly, n and We increases skin friction and heat transfer rate in cases of the stretching sheet, whereas the opposite behavior is noted with an increase in M^2. The current study provides meaningful results for industrial and engineering sectors in which stretching and shrinking sheets are involved. Furthermore, this study can be extended in the future to encompass more physical effects, such as thermophoresis, Brownian motion, nonlinear thermal radiation, chemical reaction, slip, or convective effects at boundary.

Author Contributions: Conceptualization, M.Q. and T.A.; Methodology, M.Q.; Software, S.A.; Validation, M.Q., T.A., and S.T.S.; Formal Analysis, S.A.; Investigation, A.A.; Resources, T.A.; Data Curation, S.A. and M.Q.; Writing—original Draft Preparation, M.Q. and S.A.; Writing—review & Editing, A.A. and S.T.S; Visualization, M.I. and A.S.A.; Supervision, A.S.A. and K.H.M.; Project Administration, A.S.A. and K.H.M.; Funding Acquisition, A.S.A. All authors have read and agreed to the published version of the manuscript.

Funding: This research received no external funding.

Institutional Review Board Statement: Not applicable.

Informed Consent Statement: Not applicable.

Data Availability Statement: All data that support the findings of this study are included within the article.

Acknowledgments: The authors would like to acknowledge the financial support of Taif University Researchers Supporting Project number (TURSP-2020/162), Taif University, Taif, Saudi Arabia.

Conflicts of Interest: The authors declare no conflict of interest.

Nomenclature

μ	viscosity	ν	kinematic viscosity
P	pressure	A	unsteadiness parameter
q_w	surface heat flux	τ_w	Shear stress
Γ	The time constant	λ	constant
ρ	fluid density	a, b	constants
u, v	components of velocity	κ	thermal conductivity
x, y	spatial Cartesian coordinates	α	thermal diffusivity
U_w	Stretching surface velocity	M^2	magnetic parameter
n	Power law index	U_∞	stream velocity
ψ	stream function	C_f	skin friction coefficient
σ	Electrical conductivity	We^2	Weissenberg number
V_w	suction/injection velocity	T_∞	the free stream temperature
J	magnetic field	$R_e(x)$	local Reynolds number
η	similarity variable	Pr	Prandtl number
B	stretching/ shrinking parameter	T	Fluid temperature
Nu_x	local Nusselt number	S	Suction parameter

References

1. Sakiadis, B.C. Boundary-layer behavior on continuous solid surfaces: I. Boundary-layer equations for two-dimensional and axisymmetric flow. *J. AIChe* **1961**, *7*, 26–28. [CrossRef]
2. Crane, L.J. Flow past a stretching plate. *Z. Fur Angew. Math. Und Phys.* **1970**, *21*, 645–647. [CrossRef]
3. Gupta, P.S.; Gupta, A.S. Heat and mass transfer on a stretching sheet with suction or blowing. *Can. J. Chem. Eng.* **1977**, *55*, 744-746. [CrossRef]
4. HRasheed, U.; L-Zubaidi, A.A.; Islam, S.; Saleem, S.; Khan, Z.; Khan, W. Effects of Joule Heating and Viscous Dissipation on Magnetohydrodynamic Boundary Layer Flow of Jeffrey Nanofluid Over a Vertically Stretching Cylinder. *Coatings* **2021**, *11*, 353. [CrossRef]
5. Kalpana, G.; Saleem, S. Heat Transfer of Magnetohydrodynamic Stratified Dusty Fluid Flow through an Inclined Irregular Porous Channel. *Nanomaterials* **2022**, *12*, 3309. [CrossRef] [PubMed]
6. Hamid, M.; Usman, M.; Khan, Z.H.; Ahmad, R.; Wang, W. Dual solutions and stability analysis of flow and heat transfer of Casson fluid over a stretching sheet. *Phys. Lett. A* **2019**, *383*, 2400–2408. [CrossRef]
7. Ullah, I.; Rahim, M.T.; Khan, H.; Qayyum, M. Homotopy Analysis Solution for Magnetohydrodynamic Squeezing Flow in Porous Medium. *Adv. Math. Phy.* **2016**, *2016*, 3541512. [CrossRef]
8. Kumar, R.N.; Jyothi, A.M.; Alhumade, H.; Gowda, R.J.P.; Alam, M.M.; Ahmad, I.; Gorji, M.R.; Prasannakumara, B.C. Impact of magnetic dipole on thermophoretic particle deposition in the flow of Maxwell fluid over a stretching sheet. *J. Mol. Liq.* **2021**, *334*, 116494. [CrossRef]
9. Madhukesh, J.K.; Kumar, R.N.; Gowda, R.J.P.; Prasannakumara, B.C.; Ramesh, G.K.; Khan, M.I.; Khan, S.U.; Chu, Y. Numerical simulation of AA7072-AA7075/water-based hybrid nanofluid flow over a curved stretching sheet with Newtonian heating: A non-Fourier heat flux model approach. *J. Mol. Liq.* **2021**, *335*, 116103. [CrossRef]
10. Wang, C.Y. Stagnation flow towards a shrinking sheet. *Int. J. Non-Linear Mech.* **2008**, *43*, 377–382. [CrossRef]
11. Qayyum, M.; Khan, H.; Khan, O. Slip Analysis at fluid–solid interface in MHD squeezing flow of Casson fluid through porous medium. *Results Phys.* **2017**, *7*, 732–750. [CrossRef]
12. Raza, J. Thermal radiation and slip effects on magnetohydrodynamic (MHD) stagnation point flow of Casson fluid over a convective stretching sheet. *Propuls. Power Res.* **2019**, *8*, 138–146. [CrossRef]
13. Patel, M.; Timol, M.G. Magneto Hydrodynamic Orthogonal Stagnation Point Flow of a Power-Law Fluid Toward a Stretching Surface. *Am. Comput. Math.* **2011**, *1*, 129–133. [CrossRef]
14. Ramesh, G.K.; Roopa, G.S.; Rauf, A.; Shehzad, S.A.; Abbasi, F.M. Time-dependent squeezing flow of Casson-micropolar nanofluid with injection/suction and slip effects. *Int. Commun. Heat Mass Transf.* **2021**, *126*, 105470. [CrossRef]
15. Waini, I.; Ishak, A.; Pop, I. Unsteady flow and heat transfer past a stretching/shrinking sheet in a hybrid nanofluid. *Int. J. Heat Mass Transf.* **2019**, *136*, 288–297. [CrossRef]
16. Khan, M.; Malik, M.Y.; Salahuddin, T.; Khan, I. Numerical modeling of Carreau fluid due to variable thicked surface. *Results Phys.* **2017**, *7*, 2384–2390. [CrossRef]

17. Akbar, N.S.; Nadeem, S.; Haq, R.U.; Ye, S. MHD stagnation point flow of Carreau fluid toward a permeable shrinking sheet: Dual solutions. *Ain Shams Eng. J.* **2014**, *5*, 1233–1239. [CrossRef]
18. Raju, C.S.K.; Sandeep, N. Unsteady three-dimensional flow of Casson-Carreau fluids past a stretching surface. *Alex. Eng. J.* **2016**, *55*, 1115–1126. [CrossRef]
19. Shabnam; Mei, S.; Khan, M.S. Numerical investigation of a squeezing flow between concentric cylinders under the variable magnetic field of intensity. *Sci. Rep.* **2022**, *12*, 9148.
20. Ali, N.; Hayat, T. Peristaltic motion of a Carreau fluid in an asymmetric channel. *Appl. Math. Comput.* **2007**, *193*, 535–552. [CrossRef]
21. Nazir, U.; Saleem, S.; Nawaz, M.; Sadiq, M.A.; Alderremy, A.A. Study of transport phenomenon in Carreau fluid using Cattaneo–Christov heat flux model with temperature dependent diffusion coefficients. *Phys. A Stat. Mech. Its Appl.* **2020**, *554*, 123921. [CrossRef]
22. Nadeem, S.; Riaz, A.; Ellahi, R. Series solution of unsteady peristaltic flow of a Carreau fluid in eccentric cylinders. *Ain. Shams. Eng. J.* **2014**, *5*, 293–304. [CrossRef]
23. Khashi'ie, N.S.; Arifin, N.M.; Pop, I.; Nazar, R.; Hafidzuddin, E.H.; Wahi, N. Three-Dimensional Hybrid Nanofluid Flow and Heat Transfer past a Permeable Stretching/Shrinking Sheet with Velocity Slip and Convective Condition, Chin. *J. Phys.* **2020**, *66*, 157–171. [CrossRef]
24. Gopal, D.; Firdous, H.; Saleem, S.; Kishan, N. Impact of convective heat transfer and buoyancy on micropolar fluid flow through a porous shrinking sheet: An FEM approach. *Proc. Inst. Mech. Eng. Part C J. Mech. Eng. Sci.* **2022**, *236*, 3974–3985.
25. Bakar, S.A.; Arifin, N.M.; Khashi'ie, N.S.; Bachok, N. Hybrid Nanofluid Flow over a Permeable Shrinking Sheet Embedded in a Porous Medium with Radiation and Slip Impacts. *Mathematics* **2021**, *9*, 878. [CrossRef]
26. Rohni, A.M.; Ahmad, S.; Pop, I. Flow and heat transfer over an unsteady shrinking sheet with suction in nanofluids. *Int. J. Heat Mass Transfer.* **2012**, *55*, 1888–1895.
27. Warke, A.S.; Ramesh, K.; Mebarek-Oudina, F. Numerical investigation of the stagnation point flow of radiative magnetomicropolar liquid past a heated porous stretching sheet. *J. Therm. Anal. Calorim.* **2022**, *147*, 6901–6912. [CrossRef]
28. Elbashbeshy, E.M.A.; Bazid, M.A.A. Heat transfer over an unsteady stretching surface. *Heat Mass Transfer.* **2004**, *41*, 1–4. [CrossRef]
29. Hayat, T.; Khan, W.A.; Abbas, S.Z. Impact of induced magnetic field on second-grade nanofluid flow past a convectively heated stretching sheet. *Appl. Nanosci.* **2020**, *10*, 3001–3009. [CrossRef]
30. Khan, S.A.; Ali, B.; Eze, C.; Lau, K.T.; Ali, L.; Chen, J.; Zhao, J. Magnetic Dipole and Thermal Radiation Impacts on Stagnation Point Flow of Micropolar Based Nanofluids over a Vertically Stretching Sheet: Finite Element Approach. *Processes* **2021**, *9*, 1089. [CrossRef]
31. Waini, I.; Ishak, A.; Pop, I.; Nazar, R. Dusty hybrid nanofluid flow over a shrinking sheet with magnetic field effects. *Int. J. Numer. Method H* **2022**, *32*, 1067-1091. [CrossRef]
32. Hassanien, I.A.; Al-arabi, T.H. Non-Darcy unsteady mixed convection flow near the stagnation point on a heated vertical surface embedded in a porous medium with thermal radiation and variable viscosity. *Commun. Nonlinear Sci. Numer. Simul.* **2009**, *14*, 1366–1377. [CrossRef]
33. Nandy, S.K.; Sidui, S.; Mahapatra, T.R. Unsteady MHD boundary-layer flow and heat transfer of nanofluid over a permeable shrinking sheet in the presence of thermal radiation. *Alex. Eng. J.* **2014**, *53*, 929–937. [CrossRef]
34. Zainal, N.A.; Nazar, R.; Naganthran, K.; Pop, I. Stability analysis of MHD hybrid nanofluid flow over a stretching/shrinking sheet with quadratic velocity. *Alex. Eng. J.* **2021**, *60*, 915–926. [CrossRef]
35. Chu, Y.M.; Rehman, M.I.U.; Khan, M.I.; Nadeem, S.; Kadry, S.; Abdelmalek, Z.; Abbas, N. Transportation of heat and mass transport in hydromagnetic stagnation point flow of Carreau nanomaterial: Dual simulations through Runge-Kutta Fehlberg technique. *Int. Commun. Heat Mass Transf.* **2020**, *118*, 104858. [CrossRef]
36. Ahmed, J.; Khan, M.; Ahmad, L. Stagnation point flow of Maxwell nanofluid over a permeable rotating disk with heat source/sink. *J. Mol. Liq.* **2019**, *287*, 110853. [CrossRef]
37. Long, N.M.A.N.; Suali, M.; Ishak, A.; Bachok, N.; Arifm, N.M. Unsteady stagnation point flow and heat transfer over a stretching/shrinking sheet. *J. Appl. Sci.* **2011**, *11*, 3520–3524. [CrossRef]
38. Jakeer, S.; Reddy, P.B.A. Entropy generation on EMHD stagnation point flow of hybrid nanofluid over a stretching sheet: Homotopy perturbation solution. *Phys. Scr.* **2020**, *95*, 125203. [CrossRef]
39. Khan, U.; Zaib, A.; Bakar, S.A.; Ishak, A. Stagnation-point flow of a hybrid nanoliquid over a non-isothermal stretching/shrinking sheet with characteristics of inertial and microstructure. *Case Stud. Therm. Eng.* **2021**, *26*, 101150. [CrossRef]
40. Mousavi, S.M.; Rostami, M.N.; Yousefi, M.; Dinarvand, S.; Pop, I.; Sheremet, M.A. Dual solutions for Casson hybrid nanofluid flow due to a stretching/shrinking sheet: A new combination of theoretical and experimental models. *Chin. J. Phys.* **2021**, *71*, 574–588. [CrossRef]
41. Hayat, T.; Haider, F.; Alsaedi, A.; Ahmad, B. Entropy generation analysis of Carreau fluid with entire new concepts of modified Darcy's law and variable characteristics. *Int. Comm. Heat Mass Transf.* **2021**, *120*, 105073. [CrossRef]
42. Hussain, S.M.; Goud, B.S.; Madheshwaran, P.; Jamshed, W.; Pasha, A.A.; Safdar, R.; Arshad, M.; Ibrahim, R.W.; Ahmad, M.K. Effectiveness of Nonuniform Heat Generation (Sink) and Thermal Characterization of a Carreau Fluid Flowing across a Nonlinear Elongating Cylinder: A Numerical Study. *ACS Omega* **2022**, *7*, 25309–25320. [CrossRef] [PubMed]

43. Abbas, T.; Rehman, S.; Shah, R.A.; Idrees, M.; Qayyum, M. Analysis of MHD Carreau fluid flow over a stretching permeable sheet with variable viscosity and thermal conductivity. *Phys. A Stat. Mech. Appl.* **2020**, *551*, 124225. [CrossRef]
44. Raza, R.; Mabood, F.; Naz, R. Entropy analysis of non-linear radiative flow of Carreau liquid over curved stretching sheet. *Int. Commun. Heat Mass Transf.* **2020**, *119*, 104975. [CrossRef]
45. Khan, M.; Azam, M. Unsteady heat and mass transfer mechanisms in MHD Carreau nanofluid flow. *J. Mol. Liq.* **2017**, *225*, 554–562. [CrossRef]
46. Suali, M.; Long, N.M.A.N.; Arifin, N.M. Unsteady Stagnation Point Flow and Heat Transfer over a Stretching/Shrinking Sheet with Suction or Injection. *J. Appl. Math.* **2012**, *12*, 1–13. [CrossRef]